The Amplification of East Pacific Madden–Julian Oscillation Convection and Wind Anomalies during June–November

ERIC. D. MALONEY AND STEVEN K. ESBENSEN

College of Oceanic and Atmospheric Sciences, Oregon State University, Corvallis, Oregon

(Manuscript received 27 September 2002, in final form 31 March 2003)

ABSTRACT

Madden–Julian oscillation (MJO) wind and convection anomalies are locally amplified over the northeast Pacific warm pool during June–November. Composite analysis using NCEP reanalysis data indicates that perturbation available potential energy (PAPE) production through the positive correlation of intraseasonal temperature and convective diabatic heating anomalies supports the local intensification of MJO-related east Pacific warm pool wind anomalies. PAPE production is maximum during periods of strong MJO convection and low-level westerly wind perturbations. PAPE is converted to perturbation kinetic energy through positive correlations between intraseasonal temperature and vertical velocity. Microwave Sounding Unit (MSU) temperature and NOAA outgoing longwave radiation data support the energy budget results derived from NCEP reanalysis.

The amplified east Pacific circulation enhances surface convergence and latent heat flux anomalies during MJO convective periods. The surface convergence anomalies have a strong frictional component. Intraseasonal surface convergence and latent heat flux anomalies are strongly correlated (greater than 0.7) with the negative outgoing longwave radiation anomalies that is associated with east Pacific MJO convective regions. Surface latent heat and convergence variations may therefore be important in modulating MJO convective anomalies over the east Pacific during June–November. Enhanced surface flux and convergence anomalies associated with an enhanced surface circulation may intensify MJO convection, thereby creating a feedback loop that leads to the further intensification of local wind and convection anomalies. Work with mesoscale or general circulation models is needed to confirm that surface latent heat and convergence variations are indeed important for modulating east Pacific MJO convection.

Enhanced MJO convection over the boreal summer east Pacific is accompanied by positive water vapor anomalies throughout the troposphere. Column precipitable water anomalies from both NASA Water Vapor Project (NVAP) and NCEP reanalysis are in phase with MJO convection anomalies over the east Pacific. These results support the observations of previous studies that the equatorial troposphere must be sufficiently moistened before significant MJO deep convection can occur. The strongest NCEP reanalysis specific humidity anomalies at lower levels are collocated with positive surface latent heat flux and surface convergence anomalies.

1. Introduction

The effects of the Madden–Julian oscillation (MJO; Madden and Julian 1994) on northeast tropical Pacific warm pool convection and winds during Northern Hemisphere (NH) summer have been previously documented (Kayano and Kousky 1999; Maloney and Hartmann 2000). The NH summer intraseasonal convective anomalies over the western Pacific Ocean are associated with an anomalous large-scale circulation that extends across the tropical Pacific Ocean to the coast of the Americas. Alternating periods of westerly and easterly low-level wind anomalies occur over the eastern Pacific Ocean in association with the MJO. MJO-related lower-tropospheric westerly wind anomalies are associated with a quasi-stationary area of enhanced convection over the east Pacific warm pool, and easterly anomalies are associated with suppressed convection. The strongest convection anomalies occur in regions of anomalous meridional shear of the low-level zonal wind to the north and east of the strongest wind anomalies (see Fig. 3). Maloney and Hartmann (2000) showed that circulation anomalies are locally amplified over the eastern Pacific during a NH summer MJO life cycle, presumably through interactions with convective heating. Periods of enhanced MJO convection and low-level westerly wind anomalies are accompanied by an increase of tropical cyclone activity over the eastern Pacific (Maloney and Hartmann 2000; Molinari and Vollaro 2000; Higgins and Shi 2001). Statistically significant variations of eastern Pacific sea surface temperature (SST) also occur during a boreal summer MJO life cycle (Maloney and Kiehl 2002a).

Recent studies have demonstrated that MJO circulation anomalies are amplified and supported against

Corresponding author address: Eric D. Maloney, College of Oceanic and Atmospheric Sciences, Oregon State University, 104 Ocean Admin. Building, Corvallis, OR 97331-5503.
E-mail: maloney@coas.oregonstate.edu

frictional dissipation due to the coincidence of positive diabatic heating anomalies and positive temperature perturbations (Salby et al. 1994; Hendon and Salby 1994; Yanai et al. 2000). Perturbation available potential energy (PAPE) is generated under such conditions, which can then be converted to perturbation kinetic energy through anomalous upward motion in the presence of warm temperature anomalies. We will examine the relationships among anomalous diabatic heating, vertical motion, and temperature over the eastern Pacific during a composite MJO life cycle to determine whether convective heating supports the local amplification of MJO-related circulation anomalies there. The intensification of the low-level circulation can have important consequences for surface quantities such as enhancement of latent heat flux and increased frictional convergence that may influence atmospheric convection.

The manner in which the local circulation over the east Pacific supports convection is an unanswered question. Maloney and Hartmann (2001) showed that periods of MJO-related westerly wind anomalies over the eastern Pacific are accompanied by anomalous surface convergence. This anomalous convergence may support convection by producing an upward flux of moisture in the boundary layer that moistens the lower troposphere (Hendon and Salby 1994; Maloney and Hartmann 1998), or may provide large-scale upward motion in the boundary layer to overcome convective inhibition (Mapes 2000; Xie and Zhang 2000). Maloney and Kiehl (2002a) showed that periods of enhanced MJO convection and strong surface westerly anomalies over the east Pacific warm pool are accompanied by positive latent heat flux anomalies. The strongest heat flux anomalies occur to the south and west of the strongest convection anomalies. The results of Raymond et al. (2003, manuscript submitted to *J. Atmos. Sci.*, hereafter RAY) from the East Pacific Investigation of Climate (EPIC) 2001 experiment also suggest that the imposition of surface wind variations by the MJO or equatorial Kelvin waves can cause east Pacific latent heat flux anomalies that influence deep convection. A wind-induced surface heat exchange mechanism related to that proposed by Emanuel (1987) may help to support anomalous east Pacific MJO convection. The east Pacific mechanism suggested here is different than that proposed by Emanuel (1987) in that the strongest intraseasonal latent heat fluxes occur in association with westerly wind anomalies imposed on a mean westerly flow, rather than with easterly anomalies imposed on a mean easterly flow. Regions of mean surface westerlies can also be found near the equator over the west Pacific and Indian Oceans during December–May. Previous studies have found that the strongest Indian and west Pacific MJO-related latent heat fluxes occur in association with surface westerly anomalies (e.g., Lin and Johnson 1996; Jones and Weare 1996), and so intraseasonal flux variations over the east Pacific may hold clues to intraseasonal variations in convection and winds across the Tropics.

The role of anomalous surface latent heat flux and convergence anomalies in forcing east Pacific boreal summer MJO convection will be examined in this paper. If convection forced by latent heat fluxes or anomalous convergence acts to strengthen the anomalous circulation through production of PAPE (and consequently perturbation kinetic energy), a positive feedback loop can be established until some process acts to weaken the circulation or convection. The relationships among east Pacific intraseasonal convection, latent heat fluxes, and the low-level circulation are similar to those described in the MJO model of Raymond (2001), where the rotational flow is of paramount importance for inducing enhanced latent heat fluxes to the south and west of convection. The Raymond (2001) model does not explicitly require mean westerly winds, however.

Previous studies have also suggested that the troposphere must be sufficiently moistened before strong MJO convection can occur (Hendon and Liebmann 1990; Bladé and Hartmann 1993; Hu and Randall 1994; Maloney and Hartmann 1998; Kemball-Cook and Weare 2001; Fuchs and Raymond 2002). The relationship between water vapor anomalies and enhanced east Pacific MJO convection will therefore be examined. Maloney and Kiehl (2002b) further showed, using a general circulation model coupled to a slab ocean, that an interactive oceanic mixed layer may be important for producing strong intraseasonal convective variability over the east Pacific. The implications of these results will be briefly discussed in the framework of the present study.

MJO-related variability in the northeast Pacific warm pool during NH summer is interesting because it predominantly lies outside of the atmospheric and oceanic equatorial waveguides and to the north of the equatorial cold tongue. Although boreal summer east Pacific variability on MJO timescales is strongly correlated with activity over the equatorial western Pacific (Maloney and Hartmann 2000), interactions between the east Pacific circulation and east Pacific warm pool convection clearly help amplify east Pacific intraseasonal anomalies. Statistically significant spectral peaks near 50 days in zonal winds and outgoing longwave radiation (OLR) occur in this region only during June–November (Figs. 1 and 2, seasonal cycle removed), while intraseasonal eastward-propagating variability in the equatorial waveguide is strongest during NH winter (Salby and Hendon 1994). Further, Wheeler and Kiladis (1999) showed that MJO convective variability is distinct from the dispersion curves of all equatorial trapped wave modes of shallow water theory. Explanation of the amplified intraseasonal variability over the east Pacific warm pool during NH summer may therefore give insight into the mechanisms that control intraseasonal oscillations across the Tropics during all seasons. Mechanisms that are distinct from equatorial dynamics may help regulate convection on intraseasonal timescales.

Section 2 describes the data used in this study. An

energy budget analysis during a composite boreal summer MJO life cycle over the eastern Pacific is described in section 3. Section 4 examines the role of surface convergence, latent heat fluxes, and water vapor anomalies in modulating east Pacific MJO convection. Some discussion is presented in section 5, and conclusions follow in section 6.

2. Data and compositing technique

The June–November energetics analysis presented later uses zonal winds, meridional winds, omega, temperature, and specific humidity from the National Centers for Environmental Prediction–National Center for Atmospheric Research (NCEP–NCAR) gridded (2.5° × 2.5°) reanalysis dataset during 1979–2001 (Kalnay et al. 1996). Data are used at 12 pressure levels between 1000 and 100 hPa, with the exception of specific humidity that is available only to 300 hPa. Results are subject to the assumption that the reanalysis product produces realistic fields over the eastern tropical Pacific Ocean. The specific humidity field is particularly sensitive to the model parameterizations used to construct the reanalysis dataset due to the lack of high-resolution humidity data in the east Pacific region. Heat and moisture budget analyses are also sensitive to errors in omega. Surface latent heat flux from NCEP reanalysis is used to diagnose latent heat flux anomalies during a composite MJO life cycle. These data were also used in Maloney and Kiehl (2002a) to examine MJO-related intraseasonal heat flux variations. NCEP reanalysis surface pressure is used in calculating the meridional flow that results from a balance among the zonal pressure gradient force, the Coriolis force, and turbulent drag over the tropical oceans (Holton 1992).

We utilize several independent datasets to verify that results derived from the NCEP reanalysis data are at least qualitatively correct. Column-integrated, National Aeronautics and Space Administration (NASA) Water Vapor Project (NVAP) precipitable water data from 1988–97 are used as a check on intraseasonal anomalies in NCEP water vapor (Randel et al. 1996). Microwave Sounding Unit (MSU) upper-tropospheric temperatures (channels 3/4; Spencer et al. 1990) from 1979–95 are used to independently verify results related to PAPE production as derived from the NCEP reanalysis data. The National Oceanic and Atmospheric Administration (NOAA) interpolated gridded OLR product is used throughout the paper as a proxy for atmospheric convection (Liebmann and Smith 1996). Future work with scatterometer data (e.g., Chelton et al. 2000) and Tropical Atmosphere Ocean buoy array data may be needed to validate the surface fields from NCEP reanalysis. A very interesting dataset has also recently been collected on the ship *Ron Brown* by C. Fairall during EPIC 2001 and may help validate some of the surface flux data.

The MJO compositing index is constructed in an identical manner to that described in Maloney and Kiehl (2002a). Except for a change in the numbering of MJO phases, the Maloney and Kiehl (2002a) compositing method follows that in Maloney and Hartmann (1998). The two leading empirical orthogonal functions (EOFs; Kutzbach 1967) of the 30–90-day equatorial (5°N–5°S averaged) 850-mb zonal wind over all longitudes form a quadrature pair that captures eastward-propagating MJO variability in the Tropics. The structure of the leading EOFs are very similar to those shown in Fig. 1 of Maloney and Hartmann (1998) that were derived using

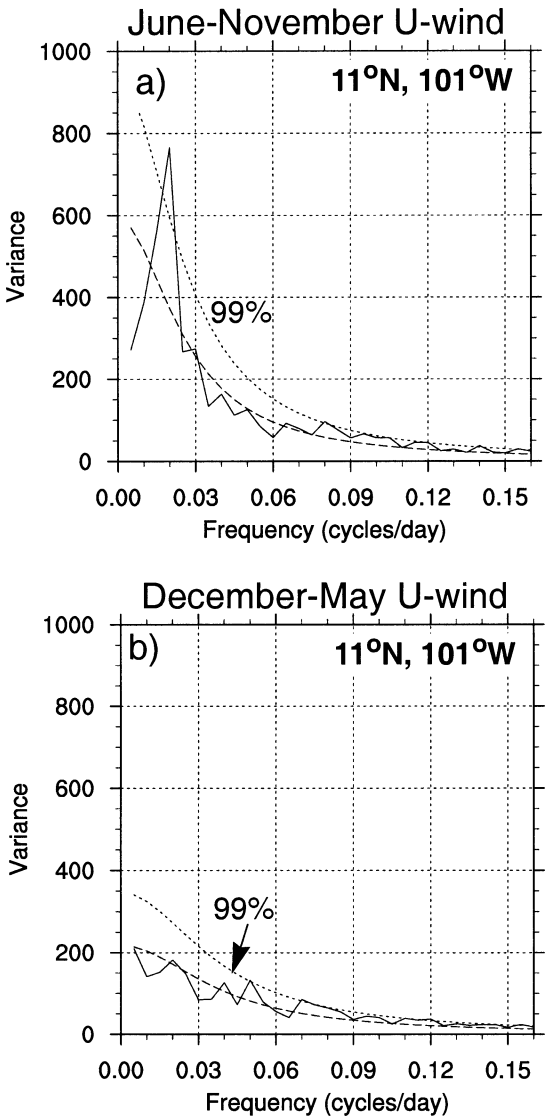

FIG. 1. Power spectra of NCEP–NCAR reanalysis 850-mb zonal wind (1979–2001) for a 5° by 5° averaging box centered at 11°N, 101°W for (a) Jun–Nov and (b) Dec–May. Spectra shown are the average of 23 spectral estimates during Jun–Nov and 22 spectral estimates during Dec–May. A 5% cosine taper was applied to the ends of each individual time series before the spectrum was computed. Long dashed lines represent the red noise spectrum and short dashed lines, the upper a priori 99% confidence limit on the red noise spectrum. The effective bandwidth is 0.00474 day^{-1}. The seasonal cycle was removed before computation of the spectra.

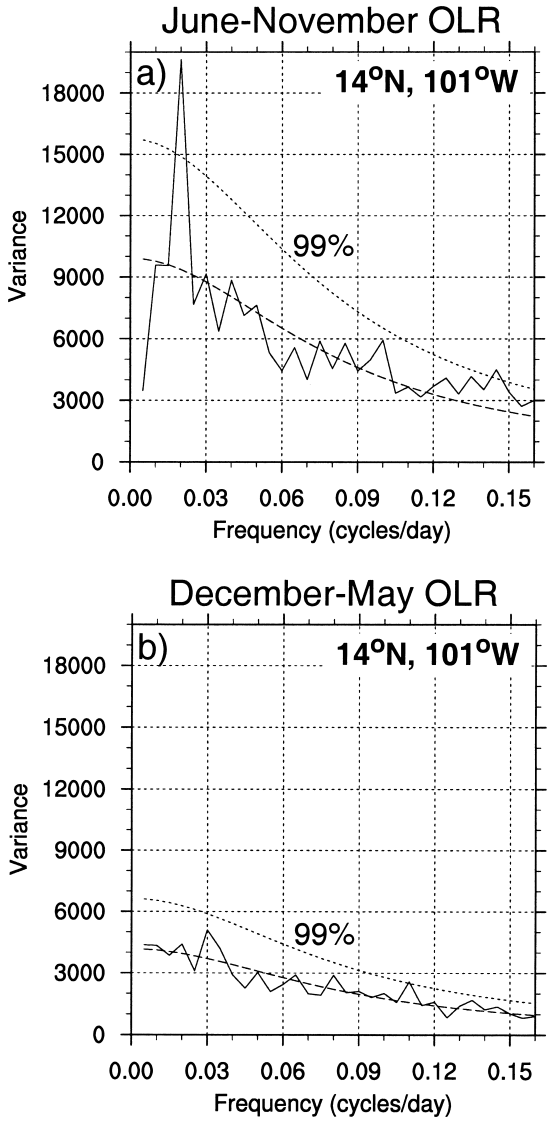

FIG. 2. Same as in Fig. 1 except for Liebmann and Smith outgoing longwave radiation at a 5° by 5° averaging box centered at 14°N, 101°W.

data from 1979 to 1995. The leading EOFs are significantly different from the others based on the criterion of North et al. (1982). The MJO index used in this paper is a linear combination of the principal components of the first two EOFs. The index has zero mean. Key events are determined by selecting periods when strong negative deviations of the index ($<-1\sigma$) occur. Results are similar if positive deviations of the index are used to select events. Negative deviations of the index represent westerly 850-mb wind anomalies over the eastern Pacific and easterly 850-mb wind anomalies over the Indian and western Pacific Oceans. Forty-four key events during June–November of 1979–2001 are selected using the criterion noted above. Nine phases are then assigned for each event, choosing phase 5 as the time of the strongest negative value of the index, when east Pacific MJO 850-mb westerly anomalies are near their peak. Phases 1 and 9 represent positive peaks of the index before and after phase 5, respectively, when MJO-related east Pacific wind anomalies are strong easterly. Phases 3 and 7 represent zero crossings of the index, and the other four phases fill in midway between the others already assigned. Results do not significantly differ if phase 5 denotes the time of peak easterly anomalies. The average time between phases is approximately 5 days. An average is taken over all 44 events to demonstrate composite behavior during a June–November MJO life cycle. See Maloney and Kiehl (2002a) and Maloney and Hartmann (1998) for more details on the compositing technique.

Intraseasonal fields throughout the paper are constructed using a linear nonrecursive filter with half-power points at 30 and 90 days. Results are not sensitive to reasonable variations in the size of the bandpass window. Budget analyses were conducted using fields high-pass filtered to 90 days in order to retain cross-frequency interactions.

3. Analysis of east Pacific PAPE generation

Figure 3 shows intraseasonal 1000-mb wind and OLR anomalies over the eastern Pacific during phases 2–9 of a composite June–November MJO life cycle. Phases are approximately 5 days apart. This figure is used as a reference when discussing wind and convection anomalies throughout this paper. A more thorough discussion of the east Pacific composite MJO life cycle is contained in Maloney and Kiehl (2002a). Enhanced convection peaks over the eastern Pacific (north of 10°N) during phases 5 and 6 in association with strong surface westerly wind anomalies centered near 10°N, and suppressed convection peaks during phases 1 (not shown) and 2 in association with surface easterly anomalies. A local intensification of the anomalous atmospheric circulation occurs over the eastern Pacific during phase 5, although low-level wind anomalies of the same sign extend westward across the Pacific. Phase-5 wind anomalies in the westernmost equatorial Pacific are of opposite sign to those in the east Pacific (not shown). We will now determine whether convective heating does indeed intensify the local atmospheric circulation over the east Pacific through generation of PAPE and subsequent conversion to perturbation kinetic energy (PKE).

Perturbation thermodynamic and moisture equations that can be used to diagnose the anomalous tropical diabatic heating field associated with MJO convection variations are developed in Yanai et al. (1973) and Lau and Lau (1992). The perturbation apparent heat source Q_1' that will be used to describe MJO-related diabatic heating of the eastern tropical Pacific atmosphere is approximately given by

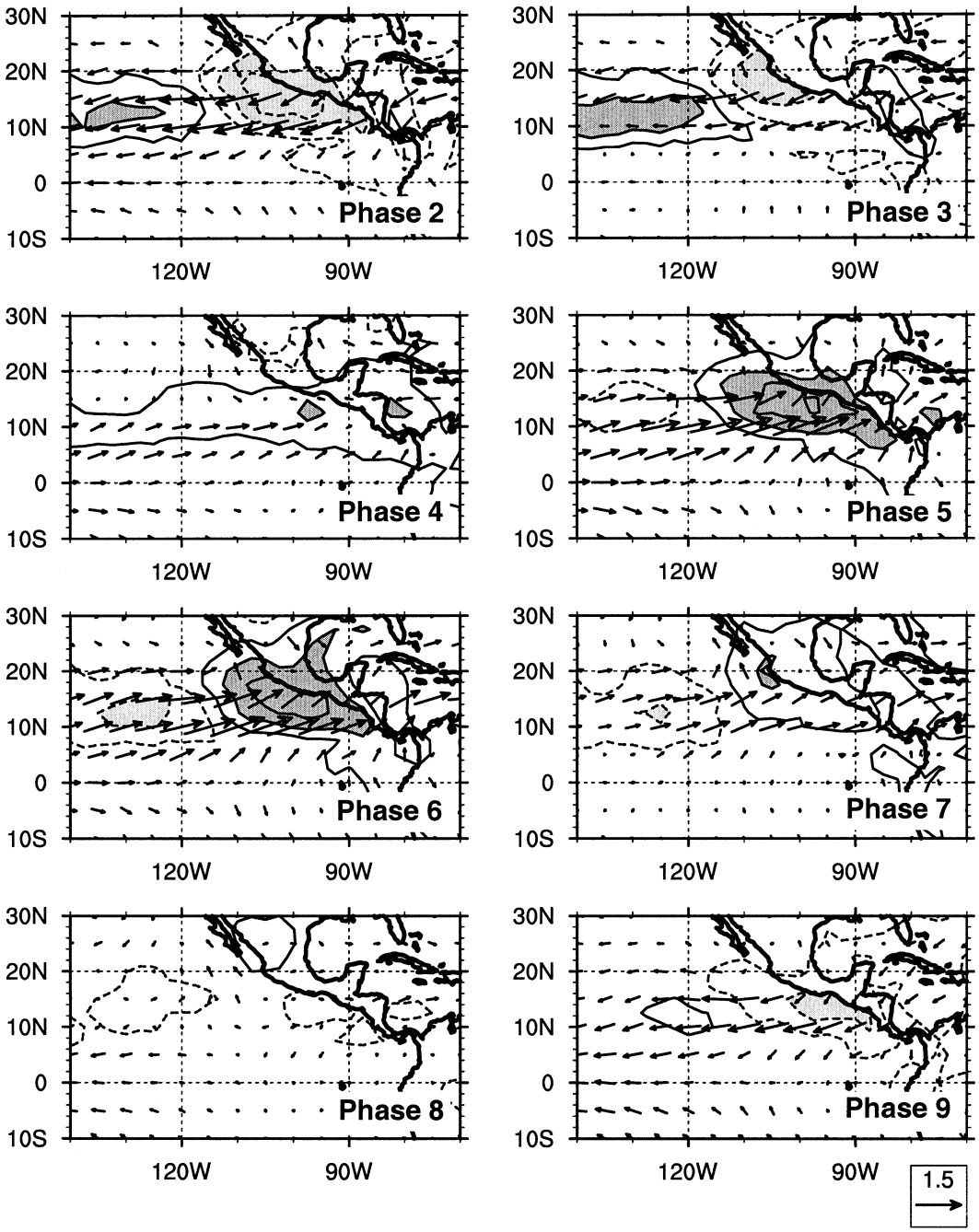

FIG. 3. Jun–Nov composite MJO 1000-hPa wind and OLR anomalies as a function of phase. OLR contours are plotted every 4 W m^{-2}, starting at 2 W m^{-2}. Negative values are solid. Values less (greater) than -6 W m^{-2} ($+6$ W m^{-2}) are dark (light) shaded. The reference wind vector is located at the bottom right.

$$Q_1' \approx c_p \frac{\partial}{\partial t} T' - c_p(\omega' \overline{\sigma} - \mathbf{V}_h' \cdot \nabla_h \overline{T}), \qquad (1)$$

where $\sigma = (RT/c_p p) - (dT/dp)$, c_p is the specific heat at constant pressure, $\mathbf{V}_h$ is the horizontal velocity vector, and ∇_h is the horizontal gradient operator. The parameter R is the gas constant for dry air. Terms related to advection by the mean and perturbation flows are negligible and not included in (1). The primed quantities on the right-hand side of (1) represent high-pass filtered fields derived using a filter with a half-power point at 90 days. The filter retains subseasonal perturbations associated with the MJO. Zonal means are not removed from the filtered fields in this study. It is not clearly appropriate to remove zonal means in the case of a localized enhancement of MJO convection and winds

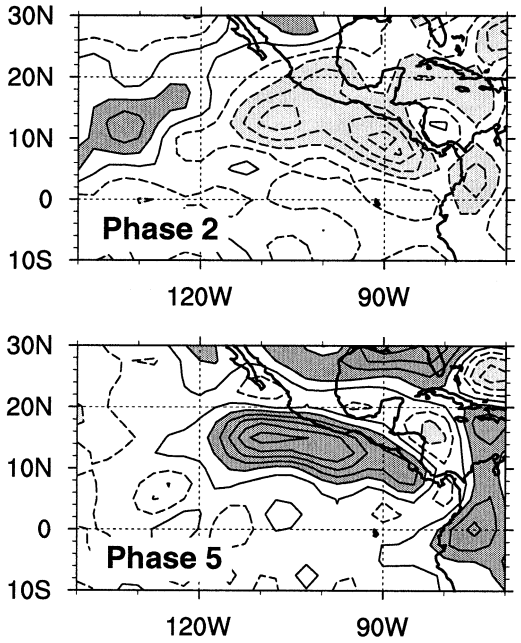

FIG. 4. Vertically averaged apparent heat source (Q_1') for phases 2 and 5 of a composite MJO life cycle. Contour interval is 0.24×10^{-2} m^2 s^{-3}, starting at 0.12×10^{-2} m^2 s^{-3}. Values greater (less) than 0.36×10^{-2} m^2 s^{-3} (0.36×10^{-2} m^2 s^{-3}) are dark (light) shaded.

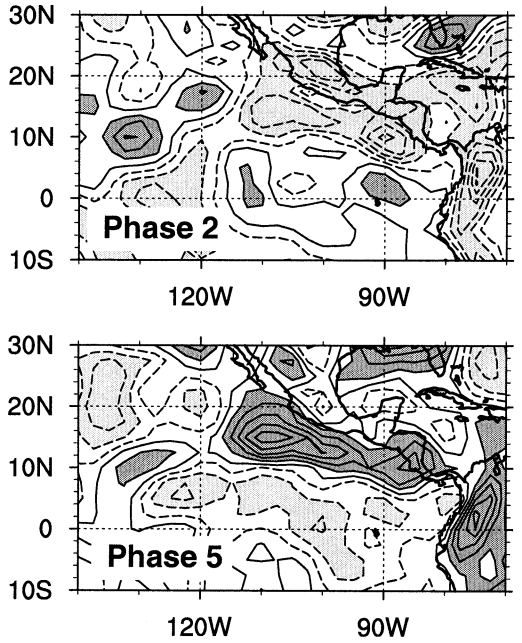

FIG. 5. Same as in Fig. 4 except for vertically averaged apparent moisture sink (Q_2').

over the eastern Pacific, outside of the equatorial waveguide. Results are very similar if zonal means are removed from all perturbation fields, however. Quantities with overbars are taken to represent the average of a field over the nine phases of an individual MJO event. Results are insensitive to the exact means by which the basic-state flows are computed. A clear scale separation between the perturbation quantities and the background-state quantities exists. The parameter Q_1' as formulated here is the sum of all diabatic heating terms, and not just latent heat release associated with deep convection. For example, radiative processes, sensible heating, and frictional heating are included in Q_1'. The perturbation apparent moisture sink Q_2' will be used to help diagnose where condensational drying is occurring over the east Pacific during MJO events. The parameter Q_2' can be approximated by

$$Q_2' \approx -L\frac{\partial}{\partial t}q' - L\left(\omega'\frac{\partial}{\partial p}\overline{q} + \mathbf{V}_h' \cdot \nabla_h \overline{q}\right), \qquad (2)$$

where L is the latent heat of condensation at 0°C. Collocation of Q_2' with Q_1' can help determine where diabatic heating processes are dominated by latent heat release.

The vertical average of a quantity $A(p)$ will be denoted by $\langle A \rangle$ throughout the remainder of this paper. This notation is consistent with that of Lau and Lau (1992). Composite fields are created by averaging over all MJO events.

Composite $\langle Q_1' \rangle$ is displayed in Figure 4 for phases 2 and 5 of a June–November MJO life cycle. Phases 2 and 5 represent the periods of peak suppressed and enhanced convection over the east Pacific, respectively. The vertically averaged diabatic heating anomalies are consistent with the location of the east Pacific OLR anomalies, a proxy for convective heating variations (Fig. 3). Phase 5 shows strong vertically averaged positive diabatic heating anomalies over the east Pacific associated with MJO convection. Lesser diabatic heating maxima occur over the western Gulf of Mexico and South America. The diabatic heating maxima along the Gulf Coast do not show a good correspondence with OLR. OLR becomes an increasingly poor proxy for convection toward midlatitudes, and $\langle Q_1' \rangle$ also accounts for processes other than condensational heating such as radiative processes, sensible heating, etc. Negative diabatic heating anomalies occur over the east Pacific during phase 2. To determine whether $\langle Q_1' \rangle$ is consistent with condensation processes, $\langle Q_2' \rangle$ for phases 2 and 5 of an MJO life cycle are shown in Figure 5. The parameter $\langle Q_2' \rangle$ is generally collocated with $\langle Q_1' \rangle$ over the east Pacific during phases 2 and 5 and is of comparable magnitude, suggesting that anomalous diabatic heating variations Q_1' are dominated by precipitation processes during an MJO life cycle. Results are similar if only perturbations on the 30–90-day timescale are considered (rather than variance at all timescales less than 90 days). A good correspondence between $\langle Q_1' \rangle$ and $\langle Q_2' \rangle$ does not exist in the Gulf of Mexico.

It will now be determined whether east Pacific convective heating perturbations are positively correlated with temperature perturbations during an MJO life cy-

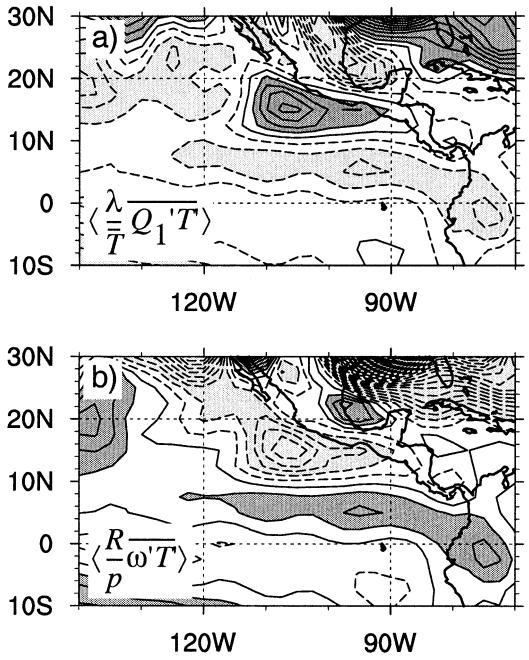

FIG. 6. MJO composite vertically averaged (a) production of PAPE due to the correlation of diabatic heating and temperature and (b) PAPE change through conversion to PKE. The contour interval is 0.8 $m^2\ s^{-2}\ day^{-1}$, starting at 0.4 $m^2\ s^{-2}\ day^{-1}$. Values greater (less) than 1.2 $m^2\ s^{-2}\ day^{-1}$ ($-1.2\ m^2\ s^{-2}\ day^{-1}$) are dark (light) shaded.

cle. Such positive correlations generate PAPE and support the local intensification of MJO circulation anomalies through the subsequent conversion of PAPE to PKE. Hendon and Salby (1994) and Yanai et al. (2000) found that MJO heating was positively correlated with warm temperature anomalies during intensification of the equatorial MJO wave signal. Following Lau and Lau (1992), generation of PAPE due to diabatic heating processes is given by

$$\left(\frac{\partial P}{\partial t}\right)_{\text{diab}} = \frac{\lambda \overline{Q_1' T'}}{\overline{T}}, \tag{3}$$

where $\lambda = \Gamma_d/(\Gamma_d - \Gamma)$. Here, Γ is the observed lapse rate and Γ_d is the dry adiabatic lapse rate. The overbar in (3) denotes an average over the nine phases of an MJO life cycle. The average in (3) is computed separately for each MJO event before composites are constructed. Primes represent 90-day high-pass fields. The destruction of PAPE due to conversion to PKE through the rising of anomalously warm air parcels is given by

$$\frac{\partial K}{\partial t} = \frac{R\overline{T'\omega'}}{p}. \tag{4}$$

Figure 6a displays composite vertically averaged PAPE generation by diabatic heating perturbations during a MJO life cycle. PAPE generation over the east Pacific maximizes within the region of strong MJO OLR variations (cf. Fig. 3). MJO convection therefore provides an energy source for the local intensification of the anomalous atmospheric circulation over the eastern Pacific. The vertically averaged PAPE generation maximizes near 3.4 $m^2\ s^{-2}\ day^{-1}$. Phase 5 contributes most strongly to PAPE generation over the MJO life cycle (not shown) due to the collocation of strong positive diabatic heating and temperature anomalies. The contribution to PAPE generation during phase 5 maximizes near 6.3 $m^2\ s^{-2}\ day^{-1}$ in association with peak enhanced MJO convective heating. Contributions to PAPE production are also heightened during periods of suppressed convective heating (phases 1 and 2). Other phases (e.g., phase 3) contribute little to the generation of PAPE. An analysis considering only interactions between MJO–timescale components (30–90 day) of the total subseasonal variations produces qualitatively similar results to those presented here for the 90-day high-pass fields, although magnitudes are generally reduced. Interactions among synoptic-scale fields and MJO perturbations may complement the PAPE generation resulting from interactions among the 30–90-day components (e.g., Straub and Kiladis 2003; Maloney and Dickinson 2003). Further, compositing 30–90-day Q_1' and T' as a function of MJO phase and then computing PAPE generation over a composite MJO life cycle produces qualitatively similar results to those described in the analysis of (3). This calculation indicates that the essence of the energy transformations are captured within the composite 30–90-day MJO fields.

Figure 6b details the composite vertically averaged conversion of PAPE to PKE during an MJO life cycle (destruction of PAPE). The PAPE generated over the eastern Pacific during an MJO life cycle is almost entirely converted to PKE. These results support the observation of Maloney and Hartmann (2000) that MJO convection locally intensifies the anomalous circulation over the eastern Pacific. Contributions to the covariance are strongest during phase 5 (not shown).

The composite vertical distribution of eastern Pacific PAPE generation along 12.5°N during an MJO life cycle is shown in Fig. 7a. This latitude crosses the area of strong MJO-related convection anomalies over the eastern Pacific Ocean. PAPE generation maximizes in the middle and upper troposphere near 105°W, within the area of strongest variations in OLR over the eastern Pacific (Fig. 3). PAPE is converted to PKE in these same areas due to the positive correlation of perturbation temperature and vertical velocity (Fig. 7b). PKE gains are ultimately realized in the lower troposphere and above 250 hPa through a reorganization of the perturbation geopotential field and subsequently through the pressure work term. A calculation of the geopotential flux convergence verifies this reorganization (not shown). The largest lower-troposphere energy gains are realized where MJO-related east Pacific wind anomalies maximize near 10°N. An excellent discussion of this redistribution process can be found in Lau and Lau (1992).

As a check on the PAPE generation results derived from NCEP reanalysis, we now examine the correlation

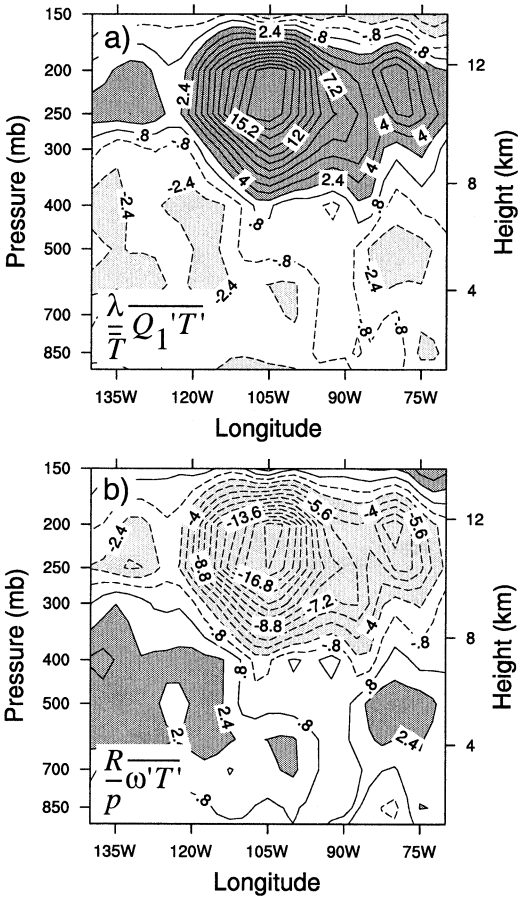

FIG. 7. MJO composite vertical cross section along 12.5°N of (a) PAPE production due to the correlation of diabatic heating and temperature and (b) PAPE change through conversion to PKE. The contour interval is 1.6 $m^2 s^{-2} day^{-1}$, starting at 0.8 $m^2 s^{-2} day^{-1}$. Values greater (less) than 2.4 $m^2 s^{-2} day^{-1}$ (-2.4 $m^2 s^{-2} day^{-1}$) are dark (light) shaded. Negative contours are dashed.

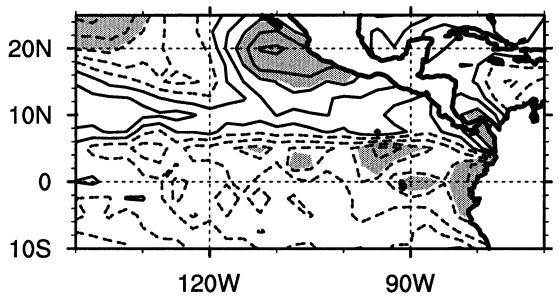

FIG. 8. Correlations between negative 30–90-day OLR anomalies and MSU level 3/4 anomalies. Correlations are computed during significant MJO events (1979–93). Contours are plotted every 0.1, starting at 0.05. Negative contours are dashed. Shading shows where correlations are significantly different from zero at the 95% confidence level, assuming 48 degrees of freedom.

between negative intraseasonal OLR anomalies and intraseasonal MSU channel 3/4 temperature anomalies during significant 1979–93 MJO events. We use the OLR anomalies as a proxy for convective heating variations. Data 40 days to either side of phase 5 of each MJO event are used in the computations. MSU channel 3/4 temperature is representative of the temperature of the deep upper-tropospheric layer between 500 and 100 hPa. A significant correlation of negative OLR anomalies and warm MSU upper-tropospheric temperature anomalies should give an indication of whether the NCEP-derived budget analyses of Fig. 6 are at least qualitatively correct. Significant correlations exist between negative OLR and MSU temperature over the east Pacific warm pool during significant MJO events (Fig. 8). These results provide independent evidence supporting the NCEP reanalysis PAPE generation results discussed earlier (e.g., Fig. 6). The strongest correlations are shifted to the northwest of the strongest PAPE generation indicated in Fig. 6. The strongest MSU temperature anomalies occur to the northwest of the strongest OLR variability (not shown), and may contribute to the higher correlations northwest of maximum convective variability. Further, OLR is an imperfect proxy for convective heating. Errors in the NCEP reanalysis fields may also contribute to the spatial phase shift. Significant negative correlations exist at 5°N in the east Pacific, consistent with the PAPE destruction indicated there in Fig. 6.

The next section will examine the implications of a locally strengthened anomalous circulation for the maintenance and growth of east Pacific MJO convection anomalies. A strengthened low-level circulation may foster the growth of more intense convection anomalies through increased surface latent heat fluxes or low-level convergence (e.g., Emanuel 1987; Hendon and Salby 1994; Waliser et al. 1999). Strengthened convection can then foster an even stronger circulation through PAPE production, creating a positive feedback loop. The role of tropospheric water vapor anomalies in modulating east Pacific MJO convection will also be addressed.

4. Control of east Pacific MJO convection by the circulation

East Pacific water vapor variations during a June–November MJO life cycle will now be examined. Because the specific humidity field in the NCEP–NCAR reanalysis product is highly dependent on the parameterizations and assumptions used in the analysis model, particularly in data-sparse regions such as the east Pacific, care must be taken when interpreting results derived from the reanalysis specific humidity field. We will therefore first compare column-integrated water vapor anomalies from NCEP reanalysis with column-integrated precipitable water anomalies from NVAP. This comparison should determine whether east Pacific column-integrated water vapor anomalies in NCEP reanalysis are at least qualitatively correct. We will also examine the vertical distribution of NCEP reanalysis water vapor anomalies. Our results are subject to the

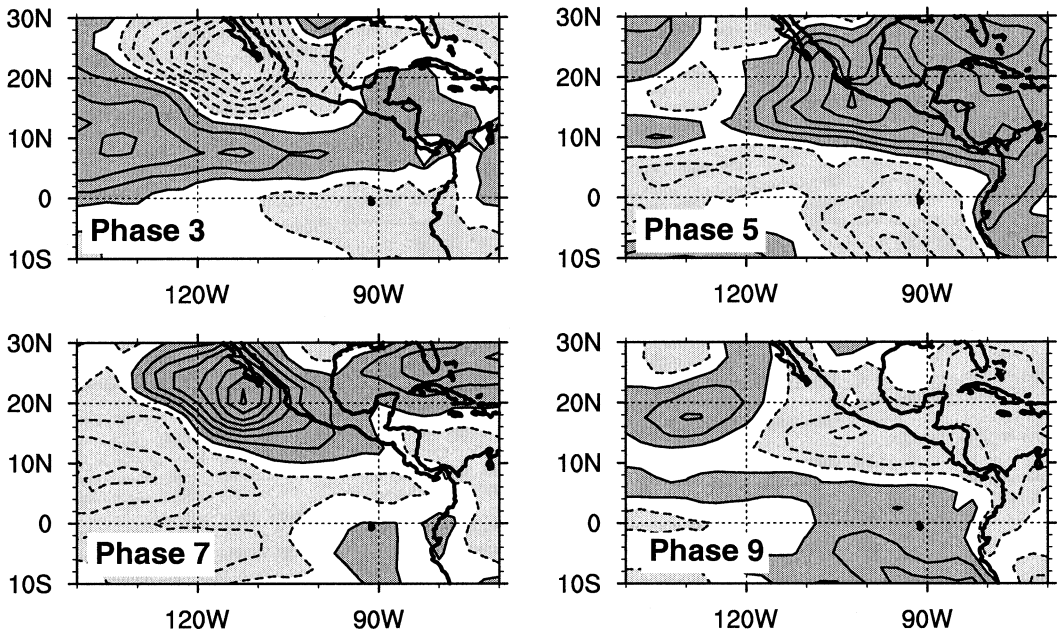

FIG. 9. Column-integrated 30–90-day NCEP water vapor anomalies for phases 3, 5, 7, and 9 of a composite MJO life cycle. Contour interval is 0.4 mm, starting at 0.2 mm. Values greater (less) than 0.2 mm (−0.2 mm) are dark (light) shaded.

assumption that the NCEP reanalysis product gives a realistic vertical distribution of specific humidity anomalies over the east Pacific during an MJO life cycle. The vertical distribution of NCEP reanalysis specific humidity may be highly sensitive to the parameterization of clouds and precipitation in the reanalysis model, and may therefore reflect errors in our understanding of the processes that control tropical clouds and precipitation. High vertical resolution specific humidity measurements may be needed to validate the NCEP reanalysis specific humidity product over the east Pacific. These caveats should be noted when considering the results shown later.

Column-integrated 30–90-day NCEP reanalysis specific humidity anomalies are plotted for phases 3, 5, 7, and 9 of a composite June–November MJO life cycle in Fig. 9. Only MJO events during 1988–97 are included in the composites, corresponding to the NVAP data record. Column-integrated NVAP precipitable water anomalies for the same phases are shown in Fig. 10. Anomalies are expressed in millimeters of precipitable water. Precipitable water anomalies look qualitatively similar between the NCEP and NVAP products. Column water anomalies peak within MJO convective areas (cf. Fig. 3) around phase 5, and a northwestward propagation of the positive anomalies occurs in both NCEP and NVAP from phase 5 to 7. Negative vapor anomalies also look qualitatively similar between NCEP and NVAP in these same regions during phases 3 and 9. The magnitudes of NVAP and NCEP anomalies in and near MJO convective regions are similar, although NCEP tends to slightly underpredict column vapor anomalies. The NCEP product tends to considerably underpredict anomaly magnitudes outside of MJO convective regions (e.g., in the intertropical convergence zone during phase 3), although the spatial distribution of the anomalies is similar to NVAP there.

A better appreciation of the phase relationship between column water vapor and MJO convection can be gained by examining the time evolution of vapor anomalies at a location of strong MJO convection. Figure 11 shows the evolution of column-integrated 30–90-day NCEP and NVAP precipitable water anomalies and negative OLR anomalies at 12.5°N, 97.5°W, near the location of strongest MJO OLR variations during an eastern Pacific MJO life cycle (see Fig. 3). The lowest OLR anomalies occur during phase 5, in conjunction with the peak in precipitable water anomalies in both the NCEP and NVAP products. The correlation between negative OLR anomalies and integrated precipitable water anomalies peaks near 0.7 at zero lag during significant MJO events (not shown). These results are consistent with previous suggestions that the atmospheric column must be sufficiently moistened for MJO convection to occur, as suggested in previous studies (e.g., Bladé and Hartmann 1993; Hu and Randall 1994; Maloney and Hartmann 1998; Kemball-Cook and Weare 2001). These results are also consistent with Fig. 1 of Fuchs and Raymond (2002) who showed that precipitation rate increases with column water content. How exactly the column gets moistened during an MJO cycle is difficult to ascertain; deep convection could itself be responsible for this moistening. NCEP reanalysis tends to underestimate column water anomalies at 12.5°N, 97.5°W by

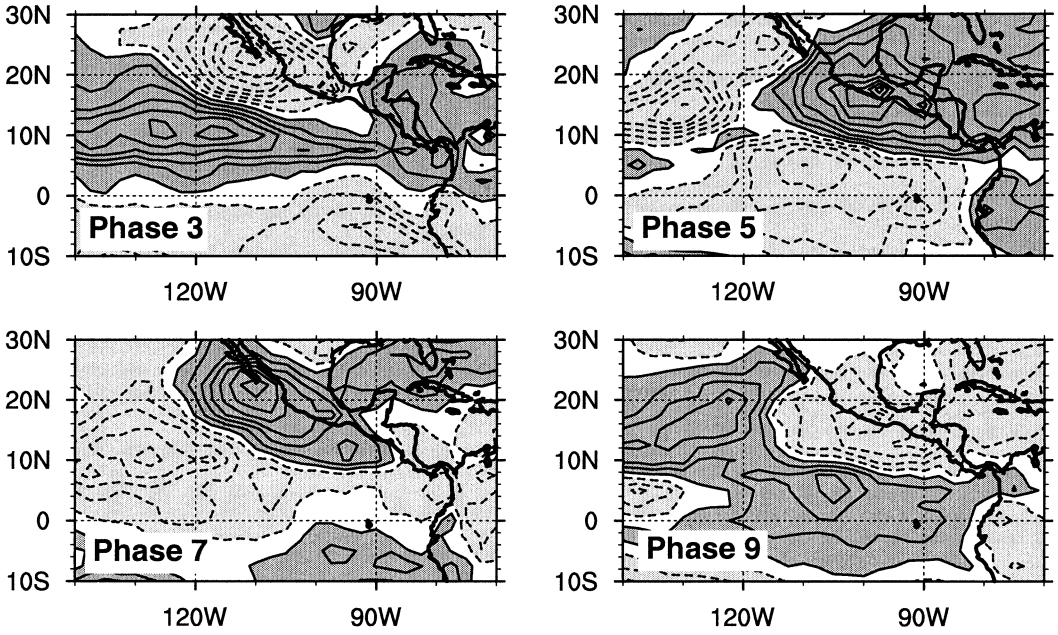

FIG. 10. Same as in Fig. 9 except for column-integrated NVAP precipitable water.

about 20% during phase 5, although the magnitude of NCEP anomalies during dry periods are quite similar to NVAP anomalies. The similarities in magnitude and phase between NCEP and NVAP precipitable water anomalies within the MJO convective region gives higher confidence that the NCEP reanalysis product produces reasonable results in this region.

Figure 12 shows vertical cross sections along 12.5°N of 30–90-day NCEP specific humidity anomalies during phases 2 and 5 of a June–November composite MJO life cycle for the entire 1979–2001 record. Results are similar for the NVAP period (1988–97). Suppressed convection periods (phase 2) are characterized by dry anomalies throughout the troposphere and enhanced convection periods are characterized by moist anomalies (phase 5). The largest percentage anomalies relative to the mean specific humidity occur in the middle and upper troposphere. The moisture variations at the midtroposphere and their relationship to convection are consistent with observations taken during the Intensive Observing Period of the Tropical Ocean Global Atmosphere Coupled Ocean Atmosphere Response Experiment that showed a moist middle troposphere accompanies deep convection periods (e.g., Lin and Johnson 1996; Brown and Zhang 1997).

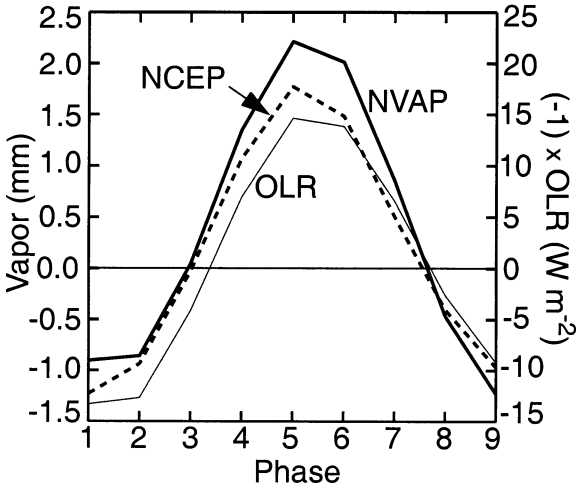

FIG. 11. The 30–90-day NCEP and NVAP column-integrated water vapor anomalies and negative OLR anomalies as a function of MJO phase at 12.5°N, 97.5°W.

Moisture variations near the surface have a very interesting structure during enhanced and suppressed convection periods (Fig. 12). A change in the sign of low-level specific humidity anomalies occurs near 115°W in both the phase 2 and phase 5 composites. Low-level moist anomalies along 12.5°N during active convective periods (phase 5) extend from 115°W to the coast of the Americas. This relationship also holds for opposite-signed anomalies during phase 2. A comparison of Fig. 12 with Figs. 13 and 14 shows that the near-surface positive specific humidity anomalies during phase 5 approximately coincide with regions of enhanced 30–90-day surface convergence and latent heat fluxes. Near-surface dry anomalies to the west of 115°W coincide with regions of suppressed latent heat flux anomalies and very small divergence anomalies. These results suggest that latent heat fluxes and convergence variations may play a role in the regulation of east Pacific MJO convection through the low-level moisture field, and thereby the moist static energy. The surface convergence anomalies occur in conjunction with anomalous cy-

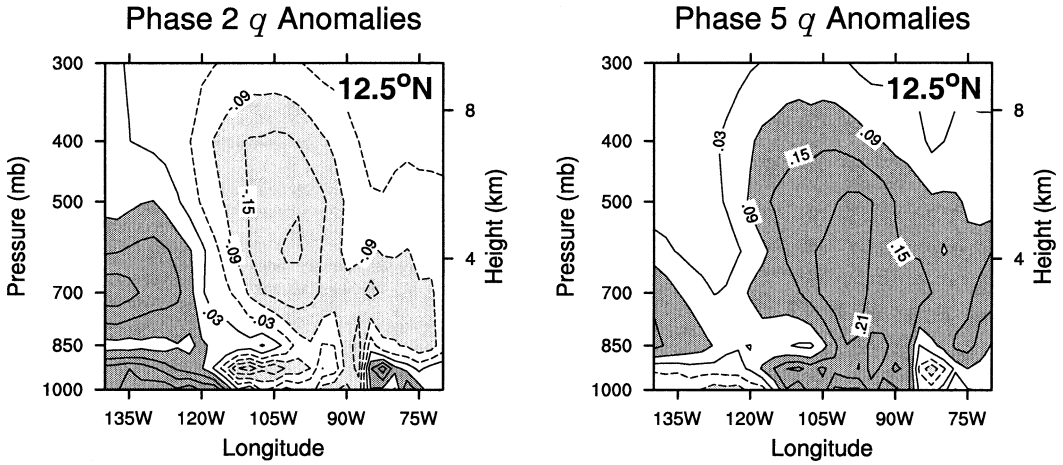

FIG. 12. Vertical cross sections of 30–90-day NCEP specific humidity anomalies along 12.5°N for phases 2 and 5 of a composite MJO life cycle. The contour interval is 0.06 g kg^{-1}, starting at 0.03 g kg^{-1}. Values greater (less) than 0.09 g kg^{-1} (-0.09 g kg^{-1}) are dark (light) shaded. Negative contours are dashed.

clonic wind shear and likely have a strong frictional component. A simple model of the meridional Ekman flow that uses only meridional NCEP reanalysis pressure gradients (e.g., Holton 1992) can reproduce to first order the magnitude and spatial extent of the east Pacific warm pool convergence anomalies given in Fig. 13. Phase-5 composites of the model 30–90-day band-passed convergence (not shown) provide a reasonable approximation to the composite shown in Fig. 13. Latent heat flux anomalies are driven primarily by the MJO surface wind anomalies added to the seasonal cycle wind field (Maloney and Kiehl 2002a). Mean June–November surface winds become easterly to the west of 115°W. If the east Pacific anomalous low-level circulation were to be intensified by diabatic heating, then surface latent heat flux and convergence anomalies would be expected to increase, potentially intensifying the convective diabatic heating anomalies.

Figure 15a shows correlations between negative OLR at 12.5°N, 97.5°W, near the location of the strongest negative OLR anomalies over the east Pacific during an MJO life cycle, and surface latent heat and convergence anomalies at 12.5°N, 97.5°W during significant MJO events. Data 40 days to either side of phase 5 of each MJO event are used in the computations. Dashed horizontal lines show where correlations are statistically significant at the 95% confidence level. Negative OLR at the location of the greatest convection anomalies is correlated with surface convergence at greater than 0.7, suggesting that surface convergence may play an important role in supporting convection during east Pacific MJO events. Convergence is nearly in phase with negative OLR anomalies at 12.5°N, 97.5°W. Maloney and Hartmann (1998) found that positive west Pacific equatorial surface convergence anomalies lead MJO convection by 5 days or more. Surface convergence occurs to the east of convection in the west Pacific due to frictional convergence into a Kelvin wavelike surface trough. Since MJO convection in the east Pacific is primarily outside of the equatorial waveguide, the phase relationship between convection and convergence are different here. Anomalous vertical velocity within MJO convective regions increases most rapidly below 900

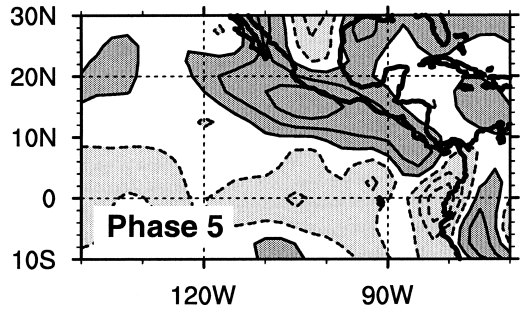

FIG. 13. The 30–90-day 1000-hPa convergence anomalies during phase 5 of a composite MJO life cycle. Contour interval is 0.4 $\times$ 10^{-6} s^{-1}, starting at 0.2 $\times$ 10^{-6} s^{-1}. Values greater (less) than 0.2 $\times$ 10^{-6} s^{-1} (-0.2 $\times$ 10^{-6} s^{-1}) are dark (light) shaded. Negative contours are dashed.

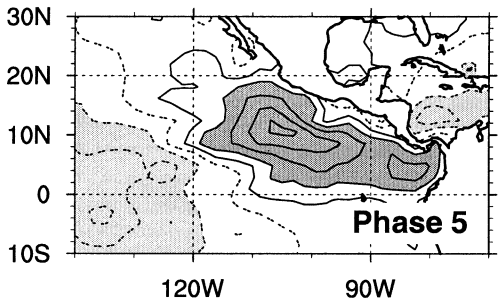

FIG. 14. The 30–90-day surface latent heat flux anomalies during phase 5 of a composite MJO life cycle. Contour interval is 4 W m^{-2}, starting at 2 W m^{-2}. Values greater (less) than 6 W m^{-2} (-6 W m^{-2}) are dark (light) shaded. Negative contours are dashed.

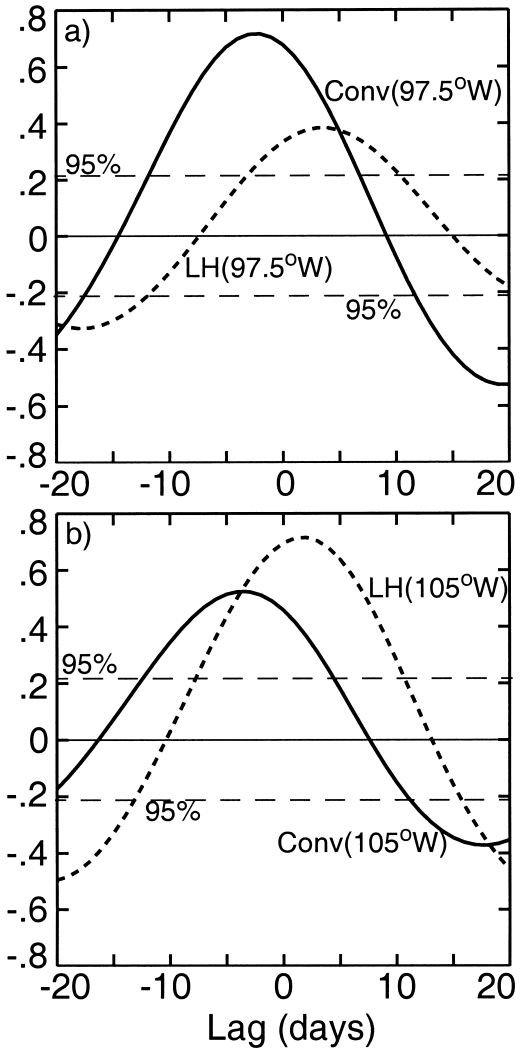

FIG. 15. Lag correlations between negative OLR anomalies at 12.5°N, 97.5°W and surface latent heat flux (LH) and convergence anomalies (Conv) at (a) 12.5°N, 97.5°W and (b) 12.5°N, 105°W. Correlations are computed during significant MJO events. A positive lag means that negative OLR (convective) anomalies lead. Dashed horizontal lines show where correlations are significantly different from zero at the 95% confidence level, assuming 86 degrees of freedom.

mb (not shown), indicating that lower-tropospheric convergence may be a major contributor to the convective mass flux. Correlations of negative OLR with collocated latent heat fluxes are significant, but considerably lower than with convergence. This suggests that collocated latent heat flux variations may not be as important as surface convergence for supporting MJO convection at 12.5°N, 97.5°W.

The preceding results do not imply that eastern Pacific latent heat fluxes are unimportant for influencing boreal summer MJO convection at 12.5°N, 97.5°W. Figure 15b shows correlations between negative OLR at 12.5°N, 97.5°W and surface latent heat and convergence anomalies at 12.5°N, 105°W, near the location of strongest east Pacific latent heat flux anomalies (Fig. 14). Latent heat fluxes at 12.5°N, 105°W are strongly correlated (greater than 0.7) with negative OLR at 12.5°N, 97.5°W. Figure 3 shows OLR anomalies at 12.5°N, 97.5°W to be downwind of 12.5°N, 105°W heat flux anomalies, with respect to intraseasonal wind perturbations. Strong westerly surface wind anomalies during phase 5, in association with mean westerly surface winds over the east Pacific warm pool during June–November (not shown), lead to an enhanced westerly flow during convectively active periods of an MJO life cycle (see Maloney and Hartmann 2001). These westerly anomalies are accompanied by positive latent heat flux anomalies, which may be communicated to convective regions to the east by the westerly surface flow. Variations in the specific humidity deficit between the ocean surface and near-surface air can also influence latent heat flux anomalies. Further analysis indicates that east Pacific MJO-related specific humidity variations contribute negligibly to the surface flux anomalies. During phase 5, positive near-surface specific humidity anomalies (Fig. 12) and weak SST anomalies (Maloney and Kiehl 2002a) contribute to a specific humidity deficit that very weakly opposes the observed positive latent heat flux anomalies in the east Pacific. The surface latent heat flux is anomalously low to the west of 115°W, where weak positive OLR anomalies occur in phases 5 and 6. These negative latent heat flux anomalies correspond to a region of surface westerly intraseasonal wind anomalies added to easterly seasonal-cycle winds (Maloney and Kiehl 2002a). These results suggest that a wind-induced surface heat exchange mechanism, related to that proposed by Emanuel (1987), may help support boreal summer MJO convection over the east Pacific. The relationship among east Pacific MJO convection, latent heat fluxes, and the low-level circulation is similar to that described in the MJO model of Raymond (2001), where the rotational flow is of paramount importance for inducing enhanced latent heat fluxes to the south and west of convection. However, the Raymond (2001) model does not explicitly require mean westerly winds, and cloud–radiative feedbacks are also needed for maintaining MJO convection.

RAY found that periods of westerly wind anomalies near 95°W during EPIC were accompanied by positive latent heat flux anomalies and enhanced convection, consistent with the results found here. In fact, the surface latent heat flux explained about 40% of the variance of deep convection over the Mexican warm pool during EPIC. RAY suggest that meridional variations in the flow are important for causing the latent heat flux variations observed. Further analysis using NCEP reanalysis winds and fluxes indicates that intraseasonal zonal wind anomalies dominate east Pacific surface flux variations near 10°N in our MJO composites, whereas meridional flow variations are of comparable importance to zonal flow variations in forcing flux anomalies near 5°N. These results deserve to be validated with data

from the EPIC experiment. The MJO index used our study (see section 2) does indicate significant MJO activity during the EPIC time period (September–October 2001). OLR-based indices also indicate significant MJO variability during EPIC (M. Wheeler 2003, personal communication). Data collected during EPIC should provide a useful tool for validating some of the surface flux results derived here using NCEP reanalyses.

We should also note that although latent heat flux anomalies peak over the eastern Caribbean Sea during phases 2 and 3, little or no enhancement of convection occurs there (Maloney and Kiehl 2002a). Thus, the results derived here for the east Pacific do not necessarily generalize to other regions. The east Pacific warm pool tends to generally be a more favorable location for convection than the Caribbean. Factors such as midtropospheric dryness (Brown and Zhang 1996; RAY), convective inhibition (e.g., Mapes 2000), and atmospheric lapse rate are also important factors for convection that we have not considered. However, it is clear from this paper that east Pacific intraseasonal convective anomalies are strongly correlated with surface convergence and latent heat flux anomalies. Surface latent heat flux and convergence variations are therefore both plausible candidates for modulating boreal summer MJO convection over the east Pacific. As discussed later, modeling work may be needed to ultimately determine the role of latent heat flux and convergence anomalies in controlling east Pacific MJO convection.

5. Discussion

The preceding results suggest a coupled feedback between convection and the low-level circulation over the east Pacific warm pool during a June–November MJO life cycle. MJO convection may strengthen the local circulation during active convective periods (Fig. 6), thereby increasing surface latent heat flux and convergence anomalies. These anomalies may then support stronger convection, creating a positive feedback loop. A modeling study using a general circulation or mesoscale model may be useful for determining the importance of surface convergence and latent heat flux anomalies to east Pacific MJO convection, since coupled feedbacks are difficult to analyze in observational data. Experiments can be conducted to decouple latent heat fluxes from surface wind variations to remove the wind-induced surface heat exchange mechanism. Maloney (2002) conducted such an experiment with a general circulation model to determine the impact of wind-induced surface heat exchange on equatorial intraseasonal variability during NH winter. Surface wind speeds were set to their climatological values in calculation of the surface latent heat flux. Equatorial model intraseasonal variability was found to be insensitive to surface flux feedbacks, although the structure of the model intraseasonal oscillation was not realistic. Similar methods for removing the effects of wind-induced surface heat exchange on model intraseasonal oscillations were used in Neelin et al. (1987) and Colon et al. (2002). Model surface drag can also be altered to gauge the effect of weakened surface frictional convergence on east Pacific convection. These experiments are highly dependent on the ability to realistically simulate boreal summer east Pacific MJO variability in a model. General circulation models (GCMs) generally do a poor job of simulating the global MJO (e.g., Slingo et al. 1996).

Another open question is the importance of SST variations in influencing east Pacific MJO convection. Maloney and Kiehl (2002a) documented a significant modulation of east Pacific SSTs during a composite MJO life cycle. The highest SSTs in MJO convective regions lead enhanced convection by about 10 days, and the strongest decline of SSTs occurs during active convective periods. SSTs decrease through enhanced surface latent heat fluxes and decreased shortwave radiation reaching the surface. These phase relationships are similar to what has been observed over the western Pacific in association with the boreal winter MJO (e.g., Zhang 1996). Magaña et al. (1999) suggest that similar phase relationships between convection and SST over the east Pacific warm pool may drive the midsummer drought that affects Mexico and Central America during July and August. The midsummer drought over the Americas is an intraseasonal oscillation that is phase-locked to the annual cycle. Although the MJO, as described by our equatorial zonal wind index, shows no relationship to the midsummer drought, it is interesting that the two phenomena involve similar interactions between convection and SST in the east Pacific.

Maloney and Kiehl (2002b) found that east Pacific intraseasonal variability in a GCM could be improved through coupling to a slab ocean model, although not all aspects of the simulation were realistic. Warm SST anomalies may help to initiate the cycle of enhanced convection over the east Pacific, in tandem with low-level westerly wind anomalies propagating into the eastern Pacific from the west. Maloney and Kiehl (2002a) showed that MJO-related eastern Pacific warm SST anomalies could force surface convergence into the east Pacific warm pool by the mechanism proposed by Lindzen and Nigam (1987). SST variations also cause east Pacific warm pool surface saturation equivalent potential temperature variations of 3°C during an MJO life cycle. Both of these mechanisms should support convection. The decline of SSTs during strong MJO convective periods may also help to terminate convection through decreased low-level moist static energy, decreased surface convergence, and a decrease in the surface latent heat flux through a reduction of surface saturation specific humidity. Propagation of easterly low-level MJO wind anomalies into the east Pacific, and drying of the midtroposphere through dry intrusions or other processes (e.g., Mapes and Zuidema 1996), may also help to weaken east Pacific MJO convection.

Another idea worth exploring is whether a localized

40–50-day periodicity in winds and precipitation (e.g., Figs. 1 and 2) can occur over the northeastern Pacific during June–November without communication with western Pacific MJO variability. Magaña et al (1999) suggest such a possibility. Results shown earlier clearly indicate that local processes act to intensify intraseasonal wind variations over the eastern Pacific during NH summer (Fig. 6). Assuming that a suitable model can be found, experiments using a GCM with a slab ocean model can be designed to isolate the east Pacific warm pool from processes over the west Pacific. Model results can be analyzed to determine if locally contained east Pacific intraseasonal oscillations can occur. A local preconditioning of the atmosphere and ocean may need to take place before strong intraseasonal convection can occur, in the spirit of the mechanisms proposed by Hendon and Liebmann (1990), Hu and Randall (1994), and Blade and Hartmann (1993) for the tropical atmosphere. A mesoscale model with an interactive ocean may also be a good candidate for such as study, because such a model would allow a better treatment of coastal topography. If a localized tropical 40–50-day periodicity in winds and precipitation can be generated outside of the equatorial waveguide through coupled interactions among convection, the large-scale circulation, and the oceanic mixed layer, important insight may be gained into MJO-timescale variability across the Tropics.

The role of topography in influencing the east Pacific MJO-related flow also deserved to be examined. Figure 13 shows that surface convergence anomalies maximize near the coast. Although a simple model of Ekman convergence assuming only meridional pressure gradients can recreate the surface convergence signal observed (as explained earlier), it may be worth examining whether topographic effects are also important. Maloney and Kiehl (2002b) showed in a GCM study that a poor resolution of topography may cause intraseasonal convection variations over the east Pacific to have more of a propagating component that in observations. Mesoscale modeling work may be useful to examine how the coast influences propagation characteristics and deviations from geostrophy on 30–60-day timescales. Orographic forcing has also been shown to be important for the initiation of tropical cyclones in this region (Zehnder 1991).

6. Conclusions

A composite life cycle of the June–November Madden–Julian oscillation (MJO) is constructed to examine the local intensification of MJO wind and convection anomalies over the northeast Pacific warm pool. Production of perturbation available potential energy (PAPE) through the positive correlation of intraseasonal temperature and convective diabatic heating anomalies supports the local intensification of east Pacific MJO-related circulation anomalies during June–November. PAPE production maximizes during periods of strong MJO convection and low-level westerly wind anomalies. Important contributions to PAPE production also occur during periods of peak suppressed convection and easterly anomalies. Production of PAPE during an MJO life cycle maximizes in the middle and upper troposphere. PAPE is converted to perturbation kinetic energy through positive correlations between intraseasonal temperature and vertical velocity. Energy budget results are derived using NCEP–NCAR reanalysis data. An analysis of MSU channel 3/4 (upper tropospheric) temperature data and OLR data (as a proxy for convective heating) supports the PAPE generation results derived from NCEP reanalysis.

The intensified local circulation enhances surface convergence and latent heat flux anomalies over the east Pacific during MJO convective periods. East Pacific intraseasonal surface convergence and latent heat flux anomalies are strongly correlated (greater than 0.7) with negative OLR anomalies within MJO convective regions. Surface latent heat and convergence variations are therefore plausible mechanisms for modulating MJO convective anomalies over the east Pacific. The strongest east Pacific warm pool latent heat flux and convergence anomalies occur in association with westerly MJO wind anomalies in the lower atmosphere. Enhanced surface flux and convergence anomalies associated with the enhanced local circulation may intensify MJO convection, thereby creating a feedback loop that leads to the further intensification of the local anomalous circulation. Modeling work is needed to isolate the importance of surface latent heat flux and surface convergence variations in modulating boreal summer east Pacific MJO convection. Modeling work may also elucidate the effects of topography on east Pacific MJO-related circulations.

Vertically integrated NCEP reanalysis and NVAP precipitable water anomalies both indicate that enhanced MJO convection over the east Pacific is accompanied by an anomalously moist equatorial troposphere. Intraseasonal NCEP and NVAP column water vapor anomalies are in phase with MJO convection anomalies over the east Pacific. These results support the assertion that the equatorial troposphere must be sufficiently moistened for significant MJO convection to occur. Positive near-surface NCEP specific humidity anomalies maximize in regions of positive surface latent heat flux and surface convergence anomalies.

Acknowledgments. The authors would like to thank Chris Bretherton and David Raymond for discussions related to the manuscript. NCEP–NCAR reanalysis data, MSU temperature data, and outgoing longwave radiation data were provided by the NOAA-CIRES Climate Diagnostics Center, Boulder, Colorado. NVAP precipitable water data were obtained from the NASA Langley Research Center Atmospheric Sciences Data Center. Eric Maloney was supported by National Science Foundation Grant ATM-0327460. Steve Esbensen was sup-

ported by National Science Foundation Grant ATM-0002322.

REFERENCES

Bladé, I., and D. L. Hartmann, 1993: Tropical intraseasonal oscillations in a simple nonlinear model. *J. Atmos. Sci.,* **50,** 2922–2939.

Brown, R. G., and C. Zhang, 1997: Variability of midtropospheric moisture and its effect on cloud-top height distribution during TOGA COARE. *J. Atmos. Sci.,* **54,** 2760–2774.

Chelton, D. B., M. H. Freilich, and S. K. Esbensen, 2000: Satellite observations of the wind jets off the Pacific coast of Central America. Part I: Case studies and statistical characteristics. *Mon. Wea. Rev.,* **128,** 1993–2018.

Colon, E., J. Lindesay, and M. J. Suarez, 2002: The impact of surface flux- and circulation-driven feedbacks on simulated Madden–Julian oscillations. *J. Climate,* **15,** 624–641.

Emanuel, K. A., 1987: An air–sea interaction model of intraseasonal oscillations in the Tropics. *J. Atmos. Sci.,* **44,** 2324–2340.

Fuchs, Z., and D. J. Raymond, 2002: Large-scale modes of a nonrotating atmosphere with water vapor and cloud–radiation feedbacks. *J. Atmos. Sci.,* **59,** 1669–1679.

Hendon, H. H., and B. Liebmann, 1990: The intraseasonal (30–50 day) oscillation of the Australian summer monsoon. *J. Atmos. Sci.,* **47,** 2909–2923.

——, and M. L. Salby, 1994: The life cycle of the Madden–Julian oscillation. *J. Atmos. Sci.,* **51,** 2225–2237.

Higgins, R. W., and W. Shi, 2001: Intercomparison of the principal modes of interannual and intraseasonal variability of the North American monsoon system. *J. Climate,* **14,** 403–417.

Holton, J. R., 1992: *An Introduction to Dynamic Meteorology.* 3d ed. Academic Press, 511 pp.

Hu, Q., and D. A. Randall, 1994: Low-frequency oscillations in radiative-convective systems. *J. Atmos. Sci.,* **51,** 1089–1099.

Jones, C., and B. C. Weare, 1996: The role of low-level moisture convergence and ocean latent heat fluxes in the Madden–Julian oscillation: An observational analysis using ISCCP data and ECMWF analyses. *J. Climate,* **9,** 3086–3104.

Kalnay, E., and Coauthors, 1996: The NCEP/NCAR 40-Year Reanalysis Project. *Bull. Amer. Meteor. Soc.,* **77,** 437–471.

Kayano, M. T., and V. E. Kousky, 1999: Intraseasonal (30–60 day) variability in the global Tropics: Principal modes and their evolution. *Tellus,* **51A,** 373–386.

Kemball-Cook, S. R., and B. C. Weare, 2001: The onset of convection in the Madden–Julian oscillation. *J. Climate,* **14,** 780–793.

Kutzbach, J. E., 1967: Empirical eigenvectors of sea-level pressure, surface temperature, and precipitation complexes over North America. *J. Appl. Meteor.,* **6,** 791–802.

Lau, K.-H., and N.-C. Lau, 1992: The energetics and propagation dynamics of tropical summertime synoptic-scale disturbances. *Mon. Wea. Rev.,* **120,** 2523–2539.

Liebmann, B., and C. A. Smith, 1996: Description of a complete (interpolated) outgoing long-wave radiation dataset. *Bull. Amer. Meteor. Soc.,* **77,** 1275–1277.

Lin, X., and R. H. Johnson, 1996: Heating, moistening, and rainfall over the western Pacific warm pool during TOGA COARE. *J. Atmos. Sci.,* **53,** 3367–3383.

Lindzen, R. S., and S. Nigam, 1987: On the role of sea surface temperature gradients in forcing low-level winds and convergence in the Tropics. *J. Atmos. Sci.,* **44,** 2418–2436.

Madden, R. A., and P. R. Julian, 1994: Observations of the 40–50-day tropical oscillation—A review. *Mon. Wea. Rev.,* **122,** 814–837.

Magaña, V., J. A. Amador, and S. Medina, 1999: The midsummer drought over Mexico and Central America. *J. Climate,* **12,** 1577–1588.

Maloney, E. D., 2002: An intraseasonal oscillation composite life cycle in the NCAR CCM3.6 with modified convection. *J. Climate,* **15,** 964–982.

——, and D. L. Hartmann, 1998: Frictional moisture convergence in a composite life cycle of the Madden–Julian oscillation. *J. Climate,* **11,** 2387–2403.

——, and ——, 2000: Modulation of eastern North Pacific hurricanes by the Madden–Julian oscillation. *J. Climate,* **13,** 1451–1460.

——, and ——, 2001: The Madden–Julian oscillation, barotropic dynamics, and North Pacific tropical cyclone formation. Part I: Observations. *J. Atmos. Sci.,* **58,** 2545–2558.

——, and J. T. Kiehl, 2002a: MJO-related SST variations over the tropical eastern Pacific during Northern Hemisphere summer. *J. Climate,* **15,** 675–689.

——, and ——, 2002b: Intraseasonal eastern Pacific precipitation and SST variations in a GCM coupled to a slab ocean model. *J. Climate,* **15,** 2989–3007.

——, and M. J. Dickinson, 2003: The intraseasonal oscillation and the energetics of summertime tropical western North Pacific synoptic-scale disturbances. *J. Atmos. Sci.,* **60,** 2153–2168.

Mapes, B. E., 2000: Convective inhibition, subgrid-scale triggering energy, and stratiform instability in a toy tropical wave model. *J. Atmos. Sci.,* **57,** 1515–1535.

——, and P. Zuidema, 1996: Radiative-dynamical consequences of dry tongues in the tropical troposphere. *J. Atmos. Sci.,* **53,** 620–638.

Molinari, J., and D. Vollaro, 2000: Planetary- and synoptic-scale influences on eastern Pacific tropical cyclogenesis. *Mon. Wea. Rev.,* **128,** 3296–3307.

Neelin, J. D., I. M. Held, and K. H. Cook, 1987: Evaporation-wind feedback and low-frequency variability in the tropical atmosphere. *J. Atmos. Sci.,* **44,** 2341–2348.

North, G. R., T. L. Bell, R. F. Cahalan, and F. J. Moeng, 1982: Sampling errors in the estimation of empirical orthogonal functions. *Mon. Wea. Rev.,* **110,** 699–706.

Randel, D. L., T. H. Vonder Haar, M. A. Ringerud, G. L. Stephens, T. J. Greenwald, and C. L. Combs, 1996: A new global water vapor dataset. *Bull. Amer. Meteor. Soc.,* **77,** 1233–1246.

Raymond, D. J., 2001: A new model of the Madden–Julian oscillation. *J. Atmos. Sci.,* **58,** 2807–2819.

Salby, M. L., and H. H. Hendon, 1994: Intraseasonal behavior of clouds, temperature, and motion in the Tropics. *J. Atmos. Sci.,* **51,** 2220–2237.

——, R. R. Garcia, and H. H. Hendon, 1994: Planetary-scale circulations in the presence of climatological and wave-induced heating. *J. Atmos. Sci.,* **51,** 2344–2367.

Slingo, J. M., and Coauthors, 1996: Intraseasonal oscillations in 15 atmospheric general circulation models: Results from an AMIP diagnostic subproject. *Climate Dyn.,* **12,** 325–357.

Spencer, R. W., J. R. Christy, and N. C. Grody, 1990: Global atmospheric temperature monitoring with satellite microwave measurements: Method and results 1979–84. *J. Climate,* **3,** 1111–1128.

Straub, K. H., and G. N. Kiladis, 2003: Interactions between the boreal summer intraseasonal oscillation and higher-frequency tropical wave activity. *Mon. Wea. Rev.,* **131,** 781–796.

Waliser, D. E., K. M. Lau, and J.-H. Kim, 1999: The influence of coupled sea surface temperatures on the Madden–Julian oscillation: A model perturbation experiment. *J. Atmos. Sci.,* **56,** 333–358.

Wheeler, M., and G. N. Kiladis, 1999: Convectively coupled equatorial waves: Analysis of clouds and temperature in the wavenumber–frequency domain. *J. Atmos. Sci.,* **56,** 374–399.

Xie, S. C., and M. H. Zhang, 2000: Impact of the convection triggering function on single-column model simulations. *J. Geophys. Res.,* **105,** 14 983–14 996.

Yanai, M., S. Esbensen, and J.-H. Chu, 1973: Determination of bulk properties of tropical cloud clusters from large-scale heat and moisture budgets. *J. Atmos. Sci.,* **30,** 611–627.

——, B. Chen, and W.-W. Tung, 2000: The Madden–Julian oscillation observed during the TOGA COARE IOP: Global view. *J. Atmos. Sci.,* **57,** 2374–2396.

Zehnder, J. A., 1991: The interaction of planetary-scale tropical easterly waves with topography: A mechanism for the initiation of tropical cyclones. *J. Atmos. Sci.,* **48,** 1217–1230.

Zhang, C., 1996: Atmospheric intraseasonal variability at the surface in the tropical western Pacific Ocean. *J. Atmos. Sci.,* **53,** 739–758.